Effect of Asynchronous GABA Release on the Oscillatory Dynamics of Inhibitory Coupled Neurons

Thomas Voegtlin and Dominique Martinez

LORIA, Campus Scientifique - BP 239, Vandoeuvre-Les-Nancy, 54506, France

Abstract

Neuronal activities often exhibit rythmic patterns, with a frequency that changes from one band to another. These oscillations can be reproduced in network models of coupled inhibitors. However, the mechanism that controls the period of the oscillations is not fully understood. Recent studies have shown that various types of inhibitory interneurons may release transmitters synchronously or asynchronously. Could this diversity explain changes in the rythm of the oscillation?

To answer this, we studied the effect of synchronous versus asynchronous inhibition, in a network of coupled inhibitory neurons. We observed that frequency and synchronization are reduced when release is asynchronous; the standard deviation of activity bursts increases linearly, while their period increases in a sublinear way. A mathematical analysis supports these observations. This suggests that the release mode of inhibition could play an important role in setting up the oscillatory frequency of inhibitory coupled neurons.

Key words: Oscillations, Synchronization, Asynchronous release

1 Introduction

Recorded electrical signals, such as electroencephalograms or local field potentials, often exhibit rythmic activity patterns. It has been shown that inhibitory interneurons play a key role in generating these rythms; oscillations may result from interactions in a purely inhibitory coupled network or from the interplay

Email addresses: Thomas.Voegtlin@loria.fr, Dominique.Martinez@loria.fr (Thomas Voegtlin and Dominique Martinez).

between inhibitory and excitatory neurons. However, the mechanism that controls the period of the oscillations is not fully understood. Analytical studies have predicted that this period linearly depends on the decay time of synaptic inhibition [4], but they fail to explain how oscillations may be generated in different frequency bands.

Recent studies have shown that there are various types of inhibitory interneurons, and suggest that this diversity could explain the changes of rythm of the oscillation [13]. More precisely, inhibitory cells may release transmitters synchronously or asynchronously [6]. Could this have an effect on the underlying rythm? To address this question, we use a simplified computational model of the mammal olfactory bulb (OB) that allows for analytic calculations.

The OB is a network mainly composed of excitatory neurons, the mitral cells (MCs), interconnected via local GABAergic neurons, the granule cells (GCs). In the mammal OB, oscillatory activity is observed both in the beta (15-30 Hz) and the gamma (40-80 Hz) frequency bands, both rythms occuring separately [3]. Experimental and modeling studies have shown that oscillations result from inhibitory feedback by granule cells. Indeed, the gamma oscillations are disrupted when the GABAergic synapses from inhibitory to excitatory cells are pharmacologically blocked [7]. However, GABAergic inhibition released by GCs and received by MCs can be asynchronous and variable across repeated trials [10,12]. In this work, we study the effects of synchronous versus asynchronous inhibition on the network oscillations and the precise synchronization of relay neurons, using computer simulations and mathematical analysis.

2 Description of the model

We consider here the quadratic integrate and fire (QIF) neuron, which is known to be a very good approximation of any type I neuron [5]. The evolution of the membrane potential V is described by :

$$C\,\frac{dV}{dt} = q(V(t) - V_T)^2 + I - I_{th} - I_{gaba}(t) \tag{1}$$

where I is a constant input current, I_{th} denotes the minimal current required for repetitive firing and I_{gaba} is a synaptic inhibitory current. In the absence of synaptic current, the QIF neuron converges to the resting potential V_{rest} when $I = 0$ and fires as soon as V reaches the threshold V_{th}, when $I \geq I_{th}$. Right after the spike, V is reset to the value V_{reset}.

Parameters were chosen as to obtain a frequency-current response similar to the MC conductance based model by [11] : $C = 0.2$ nF, $V_{rest} = -65$ mV, V_T = -60.68 mV, $q = 0.00643\ mS.V^{-1}$, I_{th}= 0.12 nA, $V_{th} = 30$ mV and V_{reset} = -70 mv.

In order to take into account the role of lateral inhibition through granule cells, we use a model of asynchronous release, inspired by [2]. On each synapse, a presynaptic spike triggers a number of GABAergic post-synaptic events. These events are triggered asynchronously, according to an exponential distribution of variance σ. The probability that a presynaptic spike at time t^f produces a post-synaptic event at time t^p is described by :

$$P_{syn}(t^p|t^f) = \sigma^{-1} e^{-\frac{t^p - t^f}{\sigma}} H(t^p - t^f) \tag{2}$$

where the Heavyside function H ensures causality. The total synaptic conductance results from the summation of these unitary synaptic events. The kinetics of unitary events are modeled by decaying exponentials :

$$g_{syn}(t) = g \sum_{t^p} e^{-\frac{t - t^p}{\tau}} H(t - t^p) \tag{3}$$

where $g = 0.5$ nS the maximum conductance resulting from a unitary synaptic event, and $\tau = 6$ ms is the synaptic time decay [9,8].

The inhibitory synaptic current $I_{gaba}(t)$ in Eq. (1) is given by

$$I_{gaba}(t) = g_{syn}(t)\,(V(t) - E_{gaba}) \tag{4}$$

where $E_{gaba} = -70$ mV is the reversal potential of the synapse.

3 Results of computer simulations

We simulated a network of 100 MCs with full connectivity. For each neuron, the transmission delay from soma to synapses was constant, equal to $\delta = 1ms$. In addition, on each synapse, each presynaptic spike triggers 10 post-synaptic events, released asynchronously according to distribution (2). In order to investigate the effects of synchronous versus asynchronous inhibition, we varied the time constant σ of the release distribution. High values of σ model the effect of asynchronous inhibition, where synaptic events may be released well after the arrival of an action potential on a synapse. Lower values of σ model the effect of synchronous inhibition.

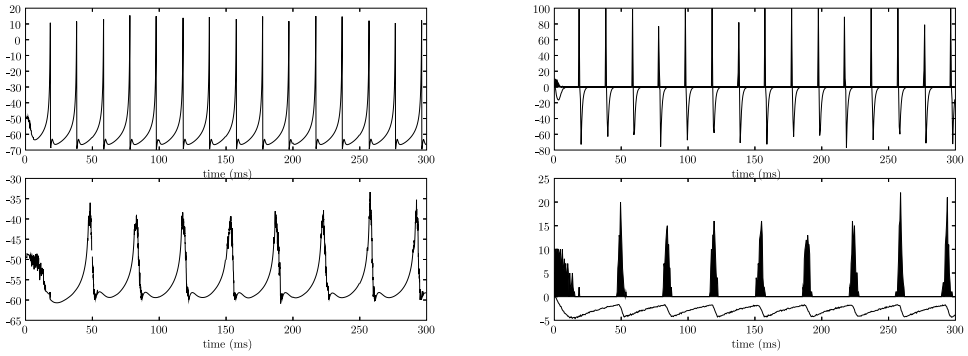

Fig. 1. Network activity over time, in two different conditions: synchronous release (top, σ=1ms) versus asynchronous release (bottom, σ=33ms). Left: Averaged membrane potential of the population (100 neurons). Right: number of action potentials in the population (plotted as positive), and global number of synaptic events (plotted as negative and rescaled). The frequency of the oscillation, measured by Fast Fourier Transform of the average membrane potential, was f=50Hz in the synchronous condition, versus f=28Hz in the asynchronous condition.

Figure 1 shows the activity histograms over time, recorded in two conditions: $\sigma = 1ms$ (top) and $\sigma = 33ms$ (bottom). It shows the evolution over time of the average membrane potential (left), action potentials and synaptic events (right). We observe that the frequency of oscillations greatly changes with σ. For $\sigma = 1ms$ we observe an oscillation at a frequency (50Hz) that is within the gamma range. We also observe that, in this range of frequencies, synaptic events are released immediately after the burst. The temporal jitter of a burst, denoted by σ_T, is very small ($\leq 1ms$), which indicates that the population fires synchronously. In contrast, for $\sigma = 33ms$, the frequency of the network is lower (28Hz, beta range). The histogram suggests that the synaptic release that follows a burst lasts much longer than the period of the oscillation, and that the resulting distribution over time of the synaptic events reaches a stable regime after a few cycles. For $\sigma = 33ms$, the fact that synaptic events may occur at any time within a cycle leads to a lower degree of synchrony (σ_T = 3.5ms).

We repeated the same experiment for different values of σ in the interval [0;50ms]. Figure 2 shows how the period of oscillations, T, and the standard deviation of the bursts, σ_T, change with σ. We see that the period T increases nonlinearly with σ. In contrast, the standard deviation σ_T increases linearly. The lowest frequency that can be obtained by increasing σ is near 25 Hz ($\sigma \approx 100ms$); for $\sigma \geq 100ms$ the network enters an asynchronous regime (data not shown). The dependency of the period of oscillations and the standard deviation of the bursts on σ will be determined mathematically in the next sections.

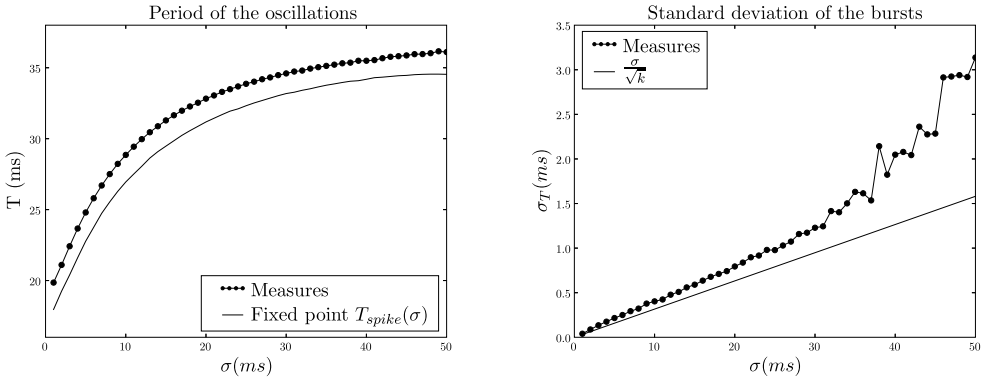

Fig. 2. Effect of the synaptic decay, σ, on the period of oscillations (left), and on the synchronization measured as the temporal dispersion (standard deviation σ_T) of the activity bursts (right). See sections 4 and 5 for explanations on the theoretical curves.

4 Standard deviation of the activity bursts

The standard deviation σ_T of the activity bursts increases with the variability of the received inhibition, as shown in Fig. 2 right. In order to characterize this dependency, we consider a neuron receiving $k >> 1$ asynchronous inhibitory synaptic events at random times t^p. Its firing time T depends on the particular arrival times of the synaptic events and, thus, the spike output jitter σ_T is a function of the synaptic input jitter σ_{t^p}. We have derived in [1] the following approximate analytical expression for the spike output jitter as a function of the variability of the received inhibition

$$\sigma_T \approx \frac{\sigma_{t^p}}{\sqrt{k}} \tag{5}$$

Note that this approximation is valid for σ_{t^p} small (see [1] for details). The arrival time of a unitary post-synaptic event is $t^p = t^f + \Delta t$. The time t^f of the pre-synaptic spike is a random variable with standard deviation σ_T. The delay $\Delta t = (t^p - t^f)$ is given by the exponential distribution with standard deviation σ (Eq. 2). Therefore, $\sigma_{t^p}^2 = \sigma_T^2 + \sigma^2$. Replacing this expression in Eq. (5) leads to

$$\sigma_T \approx \frac{\sigma}{\sqrt{k}} \tag{6}$$

Figure 2 right compares the theoretical standard deviation σ_T given by Eq. (6) to the one obtained from simulations. We see a perfect match between theoretical and experimental values when σ is small and for which Eq. (6) explains the linear dependancy between σ_T and σ. The discrepancy between theoretical and experimental σ_T values, when σ increases, is due to the approximations

made for deriving Eq. (5).

5 Period of the oscillations

In this section, we explain how frequency of the oscillations changes with σ. It should be emphasized that this change of rythm does not result from a difference in the amount of inhibition; for any value of σ, an activity burst always triggers 1000 unitary synaptic events on each neuron. Only the distribution of these events is changed. Therefore we need to investigate how the temporal distribution of inhibitory events affects the neural dynamics.

We begin by expressing the distribution of synaptic inhibitory events, in the stable regime. Given the shape of bursts in Figure 1, we make the assumption that spikes within a burst have a Gaussian distribution, of variance σ_T^2. For simplicity, we will consider that this Gaussian is centered at $t = 0$.

$$P_{spike}(t^f) = \frac{1}{\sigma_T\sqrt{2\pi}} e^{-\frac{{t^f}^2}{2\sigma_T^2}} \tag{7}$$

5.1 Synchronous synaptic release from a single activity burst

We first derive the expression of the total synaptic conductance $g_{syn}(t)$ in the limit case of a synchronous release ($\sigma = 0$ such that $t^p = t^f$ in Eq. 3):

$$g_{syn}(t) = g \sum_{t^f} e^{-\frac{t-t^f}{\tau}} H(t - t^f) \tag{8}$$

In this expression, it is possible to remove the Heavyside function, considering only causal spike times. This results in a modified summation index :

$$g_{syn}(t) = g \sum_{t_f \leq t} e^{-\frac{t-t^f}{\tau}} \tag{9}$$

On average, we have

$$g_{syn}(t) = g \int_{-\infty}^{t} P_{spike}(t^f) e^{-\frac{t-t^f}{\tau}} dt^f \tag{10}$$

This can be integrated analytically by using Eq. (7). We obtain:

$$g_{syn}(t) = g\, e^{-\frac{t-t_0}{\tau}} f(\frac{t-2t_0}{\sqrt{2}\sigma_T}) \tag{11}$$

where $t_0 = \frac{\sigma_T^2}{2\tau}$ is a time constant, and $f(x) = \frac{1}{2}(1 + erf(x))$ is a sigmoid that takes on values between 0 and 1, defined using the error function: $erf(x) = \frac{2}{\sqrt{\pi}} \int_0^x e^{-t^2} dt$.

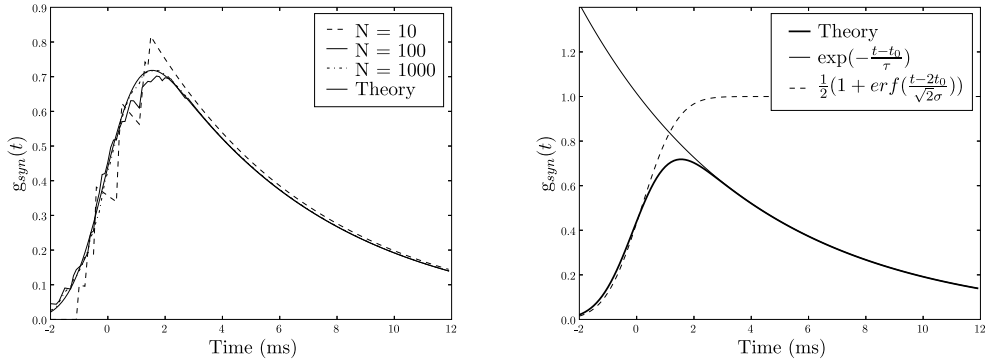

Fig. 3. Synaptic conductance $g_{syn}(t)$ resulting from a Gaussian burst of spikes, in the case of synchronous release. Left: match between theory and simulation. A burst of N spikes was centered in zero, and had a deviation σ_T=1ms. The time constant of the synapses was $\tau = 6$ ms. Right : Decomposition of $g_{syn}(t)$ as the product of a Gaussian and a sigmoid.

The total conductance given by Eq. (11) is shown in Fig. 3. It has a single maximum, and the shape of the curve depends on σ_T. For small values of σ_T, this function has the shape of a decaying exponential. For higher values of σ_T, it becomes more similar to a Gaussian.

5.2 Asynchronous synaptic release from a single activity burst

We now deal with the general case where each pre-synaptic spike triggers several post-synaptic events asynchronously. From Eq. (3), the total conductance reads

$$g_{syn}(t) = g \int_{-\infty}^{t} P_{spike}(t^f) \int_{t^f}^{t} P_{syn}(t^p|t^f) e^{-(t-t^p)/\tau} dt^p\, dt^f \tag{12}$$

Replacing $P_{spike}(t^f)$ and $P_{syn}(t^p|t^f)$ given by Eqs. (7) and (2) in the above equation leads to

$$g_{syn}(t) = g \int_{-\infty}^{t} \frac{1}{\sigma_T\sqrt{2\pi}} e^{-\frac{(t^f)^2}{2\sigma_T^2}} \int_{t^f}^{t} \sigma^{-1} e^{-\frac{t^p - t^f}{\sigma}} \; e^{-\frac{t-t^p}{\tau}} dt^p \; dt^f \tag{13}$$

The above equation can be integrated, in a similar way as in the synchronous case. This yields :

$$g_{syn}(t) = g \; \frac{1}{\frac{\sigma}{\tau} - 1} \left(e^{-\frac{t-t_1}{\sigma}} f(\frac{t - 2t_1}{\sqrt{2}\sigma_T}) - e^{-\frac{t-t_0}{\tau}} f(\frac{t - 2t_0}{\sqrt{2}\sigma_T}) \right) \tag{14}$$

with $t_0 = \frac{\sigma_T^2}{2\tau}$, $t_1 = \frac{\sigma_T^2}{2\sigma}$. The curves corresponding to the synchronous (eq. 11) and to the asynchronous case (eq. 14) are shown in figure 4. In order to draw these curves, the value of σ_T depended on σ, and it was chosen according to experimental measures from our simulations.

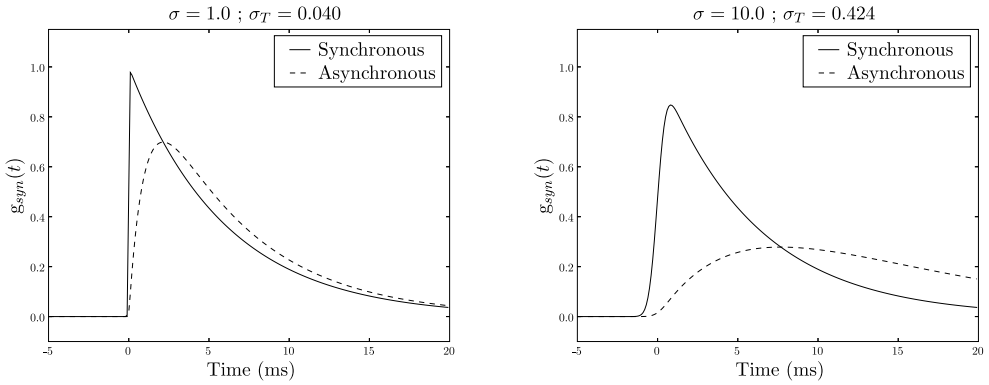

Fig. 4. Difference between the synchronous and asynchronous cases. Left : for σ small, the shape of the curve $g_{syn}(t)$ is similar to the curve in the synchronous case, but shifted to the right; g_{syn} decays with a time constant approximately equal to τ. Right : for σ higher, the shape of the curve is different; g_{syn} decays with a time constant approximately equal to σ.

5.3 Asynchronous synaptic release from several activity bursts (stable regime)

In order to study firing frequency in the stable regime, we must take into account inhibitory events from previous bursts. This is because inhibition may last longer than the period of one oscillation, especially when σ is large (see Fig. 1 right). We therefore sum the conductances computed as above :

$$G_{syn}(t) = \sum_{n=0}^{\infty} g_{syn}(t + nT) \tag{15}$$

where T denotes the period of the oscillation.

If $G_{syn}(t)$ is known, it is possible to numerically integrate Equation (1) for one single neuron, and to measure its spiking period. In turn, it is necessary to know the values of the period T and of the deviation σ_T, in order to compute $G_{syn}(t)$. In order to solve this, we used an initial estimate T_{est} in the computation of $G_{syn}(t)$, and we measured the spike time T_{spike} of a neuron initialized in the state V_{reset}. In order to take into account synaptic transmission delays, G_{syn} was shifted by the delay $\delta = 1ms$ used in the simulation. We used $\sigma_T = \sigma/\sqrt{k}$ as explained in section 4. We looked for a fixed point such that $T_{spike} = T_{est}$. This fixed point was found iteratively as follows: $T_{est}^{n+1} = 0.5(T_{est}^n + T_{spike}(T_{est}^n))$, $n \to \infty$.

The result is plotted in Figure 2 left. We observe that the period of the oscillations in our network is correctly predicted, although we observe a constant difference between theory and prediction, of about $2ms$. This discrepancy could be explained by the fact that σ_T values approximated in Equation (6) were underestimated. Nevertheless, the shape of the fixed point curve matches that of the experimentally measured period, which demonstrates that the temporal distribution of inhibitory events is a key factor for controlling the period of the oscillation.

6 Conclusion

Our results suggest that the release mode of GABA (synchronous vs. asynchronous) could play an important role in setting up the oscillatory frequency in inhibitory coupled neurons. In the mammal OB, oscillatory activity is observed both in the beta and the gamma frequency bands. Our results suggest that beta and gamma frequencies could result from synchronous and asynchronous release, respectively. Experimental studies have shown that inhibitory cells in the OB may release GABA asynchronously [10,12]. However, the transition between beta and the gamma frequencies remains to be understood. Feedback from the olfactory cortex plays a role in setting up the beta frequency, as this rythm disappears when the bulb is disconnected from the cortex. The switch from gamma to beta might result from the activation of anatomically different synapses by the olfactory cortex (e.g. lateral inhibition vs recurrent inhibition) or different interneurons.

References

[1] M. Ambard and D. Martinez. Inhibitory control of spike timing precision. *Neurocomputing*, 2006.

[2] B. Bathellier, S. Lagier, P. Faure, and P-M. Lledo. Circuit properties generating gamma oscillations in the mammalian olfactory bulb. *J. Neurophysiol.*, doi:10.1152/jn.01141.2005 26 (12), Dec. 2005.

[3] N. Buonviso, C. Amat, P. Litaudon, S. Roux, J-P. Royet, and V. Farget. Rythm sequence through the olfactory bulb layers during the time window of a respiratory cycle. *European Journal of Neuroscience*, 17:1811–1819, 2003.

[4] C.C. Chow, J.A. White, J. Ritt, and N. Kopell. Frequency control in synchronized networks of inhibitory neurons. *Journal of computational neuroscience*, 5:407–420, 1998.

[5] B. Ermentrout. Type 1 membranes, phase resetting curves, and synchrony. *Neural computation*, 8:979–1001, 1996.

[6] S. Hefft and P. Jonas. Asynchronous gaba release generates long-lasting inhibition at a hippocampal interneuron-principal neuron synapse. *Nature Neuroscience*, 8 (10):1319–1328, 2005.

[7] S. Lagier, A. Carleton, and P-M. Lledo. Interplay between local gabaergic interneurons and relay neurons generate γ oscillations in the rat olfactory bulb. *The Journal of Neuroscience*, 24:4382–4392, 2004.

[8] T.W. Margrie and A.T. Schaefer. Theta oscillation coupled spike latencies yield computational vigour in a mammalian sensory system. *J. Physiol*, 2002.

[9] Z. Nusser. Release-independent short-term facilitation on gabaergic synapses in the olfactory bulb. *Neuropharmacology*, 43:573–583, 2002.

[10] N. Schoppa, J.M. Kinzie, Y. Sahara, T.P. Segerson, and G.L Westbrook. Dendrodendritic inhibition in the olfactory bulb is driven by nmda receptors. *The Journal of Neuroscience*, 18:6790–6802, 1998.

[11] G.Y. Shen, W.R. Chen, J. Mitdgaard, G.M. Shepherd, and M.L. Hines. Computational analysis of action potential initiation in mitral cell soma and dendrites based on dual patch recordings. *J. Neurophysiol.*, 82:3006–3020, 1999.

[12] N. Urban and B. Sakmann. Reciprocal intraglomerular excitation and intra- and interglomerular lateral inhibition between mouse olfactory bulb mitral cells. *Journal of Physiology*, pages 355–367, 2002.

[13] M.A. Whittington and R.D. Traub. Interneuron diversity series: inhibitory interneurons and network oscillations in vitro. *Trends in Neurosciences*, 26 (12):676–682, 2003.